

TWO-CURRENT-SHEET RECONNECTION MODEL OF INTERDEPENDENT FLARE AND CORONAL MASS EJECTION

Y. Z. ZHANG,¹ J. X. WANG,¹ AND Y. Q. HU²

Received 2005 September 30; accepted 2005 December 13

ABSTRACT

Time-dependent resistive magnetohydrodynamic simulations are carried out to study a flux rope eruption caused by magnetic reconnection with implication in coexistent flare-CME (coronal mass ejection) events. An early result obtained in a recent analysis of double catastrophe of a flux rope system is used as the initial condition, in which an isolated flux rope coexists with two current sheets: a vertical one below and a transverse one above the flux rope. The flux rope erupts when reconnection takes place in the current sheets, and the flux rope dynamics depends on the reconnection sequence in the two current sheets. Three cases are discussed: reconnection occurs (1) simultaneously in the two current sheets, (2) first in the transverse one and then in the vertical one, and (3) in an order opposite that of case 2. Such a two-current-sheet reconnection exhibits characteristics of both magnetic breakout for CME initiation and the standard flare model. We argue that both breakout-like and tether-cutting reconnections could be important for CME eruptions and associated surface activities.

Subject headings: Sun: corona — Sun: coronal mass ejections (CMEs) — Sun: flares — Sun: magnetic fields

1. INTRODUCTION

A number of coronal mass ejections (CMEs) showed structures consistent with the ejection of a magnetic flux rope, as has been reported by Chen et al. (1997), Wood et al. (1999), and Dere et al. (1999). Therefore, magnetic flux ropes have been presumed to be typical structures in the solar corona, and their eruptions might be closely related to solar flares and CMEs (Forbes 2000; Low 2001). Many studies, both analytical and numerical, tried to explain such eruptive phenomena (Anzer 1978; Priest 1988; Forbes & Isenberg 1991; Isenberg et al. 1993; Mikić & Linker 1994; Forbes & Priest 1995; Low 1996; Wu et al. 1997; Antiochos et al. 1999; Chen & Shibata 2000; Hu & Liu 2000; Lin & Forbes 2000; Amari et al. 2000; Lin et al. 2001; Cheng et al. 2005; Török & Kliem 2005). Most of them were associated with a bipolar magnetic configuration and assumed that reconnection in the current sheet below the flux rope triggers the eruption by the so-called tether cutting of the field lines. However, observations always show complicated magnetic configurations and global coupling of different flux systems (see an example described by Wang et al. [2006] and a statistical analysis by Zhou et al. [2006]).

Two types of models are popular in the investigation of solar eruptive phenomena: the standard flare model and the magnetic breakout model. The standard flare model for magnetic explosions in eruptive flares was first proposed by Sturrock (1966) and advanced by many later studies (Hirayama 1974; Heyvaerts et al. 1977; Sturrock et al. 1984; Shibata et al. 1995; Tsuneta 1997; Shibata 1999; Chen & Shibata 2000; Moore et al. 2001). Recently, Chen & Shibata (2000) proposed an emerging flux trigger mechanism for CMEs, in which reconnection in the current sheet below the rope leads to an eruption of the CME and a cusp-shaped solar flare. All of these studies showed that a cusp structure and a two-ribbon flare occur in the lower corona and that the reconnection is tether-cutting at the internal current sheet. Another type of model is the breakout model (Antiochos et al.

1999), which involves multipolar topology and requires external magnetic reconnection to occur on the top of the sheared arcade. In their model the background field has a spherically symmetric quadrupolar configuration, rather than a simple bipolar one.

Many observations have shown that CMEs and flares are often two aspects of the same eruptive event. In a recent study (Zhang et al. 2005) we found that a double catastrophe exists for an isolated flux rope embedded in a quadrupolar background field. After the first catastrophe, the flux rope levitates in the solar corona and two current sheets coexist with the rope, a transverse one above and a vertical one below the rope. As a product of the interaction between the central and overlying arcades, the transverse current sheet represents the large-scale nature of the flux system. On the other hand, the vertical current sheet is limited to the interior of the central arcade and comes from a local interaction between small-scale bipoles. The coexistence of the two current sheets differentiates the present magnetic configuration between either the configuration of the magnetic breakout model or that of the standard flare model. In the absence of reconnection, the flux rope can levitate in the corona in equilibrium. The resulting magnetic configuration provides a preeruption magnetic topology for a potential CME and its associated surface magnetic activity and meets the requirements of the magnetic breakout and standard flare models. Once reconnection sets in across one of the two current sheets or both, an eruption of the flux rope is inevitable, which is presumably responsible for the concurrence of CMEs and flares. To explore this possibility, we take one of the force-free field solutions obtained by Zhang et al. (2005) as the initial state, which is located right after the first catastrophic point, introduce resistive dissipation in the current sheets, and examine the dynamic evolution of the flux rope system. The numerical results show both breakout and tether cutting.

We describe the time-dependent, resistive magnetohydrodynamic (MHD) equations and the solution procedures in § 2. We discuss the evolution of the flux rope system in § 3 and conclude our work in § 4.

2. BASIC EQUATIONS AND SOLUTION PROCEDURES

We use time-dependent resistive MHD simulations to study the dynamic evolution of a flux rope system in the presence of

¹ National Astronomical Observatories, Chinese Academy of Sciences, Beijing 100012, China.

² School of Earth and Space Sciences, University of Science and Technology of China, Hefei 230026, China.

resistance. For 2.5-dimensional MHD problems in spherical coordinates (r, θ, φ) , one can introduce a magnetic flux function $\psi(t, r, \theta)$ related to the magnetic field by

$$\mathbf{B} = \nabla \times \left(\frac{\psi}{r \sin \theta} \hat{\varphi} \right) + \mathbf{B}_\varphi, \quad \mathbf{B}_\varphi = B_\varphi \hat{\varphi}, \quad (1)$$

where B_φ is the azimuthal component of the magnetic field. Then the 2.5-dimensional resistive MHD equations are cast in the following form:

$$\frac{\partial \rho}{\partial t} + \nabla \cdot (\rho \mathbf{v}) = 0, \quad (2)$$

$$\begin{aligned} \frac{\partial \mathbf{v}}{\partial t} + \mathbf{v} \cdot \nabla \mathbf{v} + \frac{1}{\rho} \nabla p + \frac{1}{\mu \rho} [L\psi \nabla \psi + \mathbf{B}_\varphi \times (\nabla \times \mathbf{B}_\varphi)] \\ + \frac{1}{\mu \rho r \sin \theta} \nabla \psi \cdot (\nabla \times \mathbf{B}_\varphi) \hat{\varphi} + \frac{GM_\odot}{r^2} \hat{\mathbf{r}} = 0, \end{aligned} \quad (3)$$

$$\frac{\partial \psi}{\partial t} + \mathbf{v} \cdot \nabla \psi - \frac{1}{\mu} \eta r^2 \sin^2 \theta L\psi = 0, \quad (4)$$

$$\begin{aligned} \frac{\partial B_\varphi}{\partial t} + r \sin \theta \nabla \cdot \left(\frac{B_\varphi \mathbf{v}}{r \sin \theta} \right) + \left[\nabla \psi \times \nabla \left(\frac{v_\varphi}{r \sin \theta} \right) \right]_\varphi \\ - \frac{1}{r \sin \theta} \nabla \eta \cdot \nabla (\mu r \sin \theta B_\varphi) - \frac{1}{\mu} \eta r \sin \theta L(r B_\varphi \sin \theta) = 0, \end{aligned} \quad (5)$$

$$\frac{\partial T}{\partial t} + \mathbf{v} \cdot \nabla T + (\gamma - 1) T \nabla \cdot \mathbf{v} - \frac{\gamma - 1}{\rho} \eta j^2 = 0, \quad (6)$$

where

$$L\psi \equiv \frac{1}{r^2 \sin^2 \theta} \left(\frac{\partial^2 \psi}{\partial r^2} + \frac{1}{r^2} \frac{\partial^2 \psi}{\partial \theta^2} - \frac{\cot \theta}{r^2} \frac{\partial \psi}{\partial \theta} \right), \quad (7)$$

$$\mathbf{j} = \frac{1}{\mu} \nabla \times \mathbf{B} = -\frac{1}{\mu} r \sin \theta L\psi \hat{\varphi} + \frac{1}{\mu} \nabla \times (B_\varphi \hat{\varphi}), \quad (8)$$

ρ is the density, \mathbf{v} is the flow velocity, μ is the vacuum magnetic permeability, G is the gravitational constant, M_\odot is the mass of the Sun, T is the temperature, γ ($=1.05$) is the polytropic index, η is the resistivity, and \mathbf{j} is the current density.

The computational domain is taken to be $1 \leq r \leq 30$ in units of solar radii (R_\odot) and $0 \leq \theta \leq \pi/2$, discretized into 130×90 grid points. The grid spacing increases according to a geometrical series of common ratio 1.03 from 0.02 at the base ($r = 1$) to 0.86 at the top ($r = 30$), whereas a uniform mesh is adopted in the θ -direction. The multistep implicit scheme (Hu 1989) is used to solve equations (2)–(6). As for the boundary conditions, we use appropriate symmetrical conditions at the pole and equator and calculate the quantities at the top in terms of equivalent extrapolation except for B_φ and ψ . The magnetic field is potential above the transverse current sheet that is below the top boundary. Therefore, B_φ is set to be 0 and ψ is calculated from $j_\varphi = -r \sin \theta L\psi = 0$ at the top (see Hu et al. 2003; Hu 2004; Zhang et al. 2005).

The initial corona is assumed to be isothermal and static with $T = T_0 = 2 \times 10^6$ K and $\rho = \rho_0 = 1.67 \times 10^{-13}$ kg m $^{-3}$ at the coronal base, where T_0 and ρ_0 are taken to be the units for temperature and density, respectively. Taking a characteristic value of 0.01 for β , the ratio of gas pressure to magnetic pressure, leads to a characteristic value of $\psi_0 = (2\mu\rho_0 R T_0 R_\odot^4 / \beta)^{1/2} = 5.69 \times 10^{14}$ Wb, taken to be the unit of ψ . Other units of interest

are $B_0 = \psi_0 / R_\odot^2 = 1.18 \times 10^{-3}$ T for the field strength, $v_A = B_0 / (\mu\rho_0)^{1/2} = 2570$ km s $^{-1}$ for the velocity, $\tau_A = R / v_A = 271$ s for the time, and $j_0 = B_0 / (\mu R_\odot) = 1.35 \times 10^{-6}$ A m $^{-2}$ for the electric current density.

We choose a force-free field solution as the initial magnetic field. This solution was obtained by Zhang et al. (2005) right after the first catastrophic point, characterized by an isolated flux rope levitating in the corona and accompanied by two current sheets, a transverse one above and a vertical one below the rope. The annular magnetic flux per radian is 0.6 in units of ψ_0 , the axial magnetic flux is 0.0416 in units of ψ_0 for the flux rope, and both of them are conserved during subsequent dynamic evolutions of the flux rope system. The magnetic energy of the initial field is 1.71, which is still larger than the energy of the associated partially open field, 1.662, by 2.9% (see Zhang et al. 2005). The excess energy is obviously in favor of high-speed CMEs.

The initial field chosen above is in equilibrium in the ideal MHD regime but will certainly evolve into a dynamic state once reconnection sets in across the current sheets. The temporal evolution of the whole system depends on how reconnection occurs in the two current sheets. Three cases are treated, hereafter labeled A, B, and C, which differ in the sequence of reconnection. Reconnection starts simultaneously in the two current sheets in case A, first in the transverse current sheet and later in the vertical one in case B, and in the opposite order in case C. To control the sequence of reconnection, we introduce a critical current density for each current sheet, denoted by j_t for the transverse current sheet and j_v for the vertical one. When the current density near the transverse current sheet exceeds j_t or that near the vertical current sheet exceeds j_v , the resistivity of η is set to be 0.01, and η is set to be 0 elsewhere. Consequently, we can simply set j_t larger than the initial peak current density in the transverse current sheet to delay reconnection or smaller than the initial peak current density to start reconnection across the sheet. Note that a larger value of j_t just causes a delay of reconnection rather than prohibits it. As a matter of fact, the current density in the transverse current sheet grows with time during the rope eruption, so it may eventually exceed j_t somewhere, leading to a delayed onset of reconnection in the sheet. The same is the case for the vertical current sheet. Such an expedient measure is somewhat artificial but satisfies our purpose. Through tentative calculations, we find that the initial peak current density is 5.3 in the transverse current sheet and 22.1 in the vertical current sheet. Consequently, we choose $(j_t, j_v) = (5, 20)$ for case A, $(5, 40)$ for case B, and $(10, 20)$ for case C.

3. SIMULATION RESULTS

As mentioned in the previous section, we intend to discuss three cases, a simultaneous reconnection in the transverse and vertical current sheets for case A, a first reconnection in the transverse current sheet followed by a second in the vertical current sheet for case B, and a first reconnection in the vertical current sheet followed by a second in the transverse current sheet for case C. In each case, we use the height of the rope axis relative to the solar surface, h_a , to mark the position of the flux rope. For the initial state, we have $h_a = 1.70$.

In case A, reconnection occurs simultaneously in the transverse and vertical current sheets. Figures 1a–1c show the magnetic configuration at three separate times, along with the temperature distribution in color. Figure 1a corresponds to the initial state, and resistive dissipation is switched on in both current sheets at $t = 0$. Since then, high temperature appears in the current sheet regions because of reconnection, and the flux rope

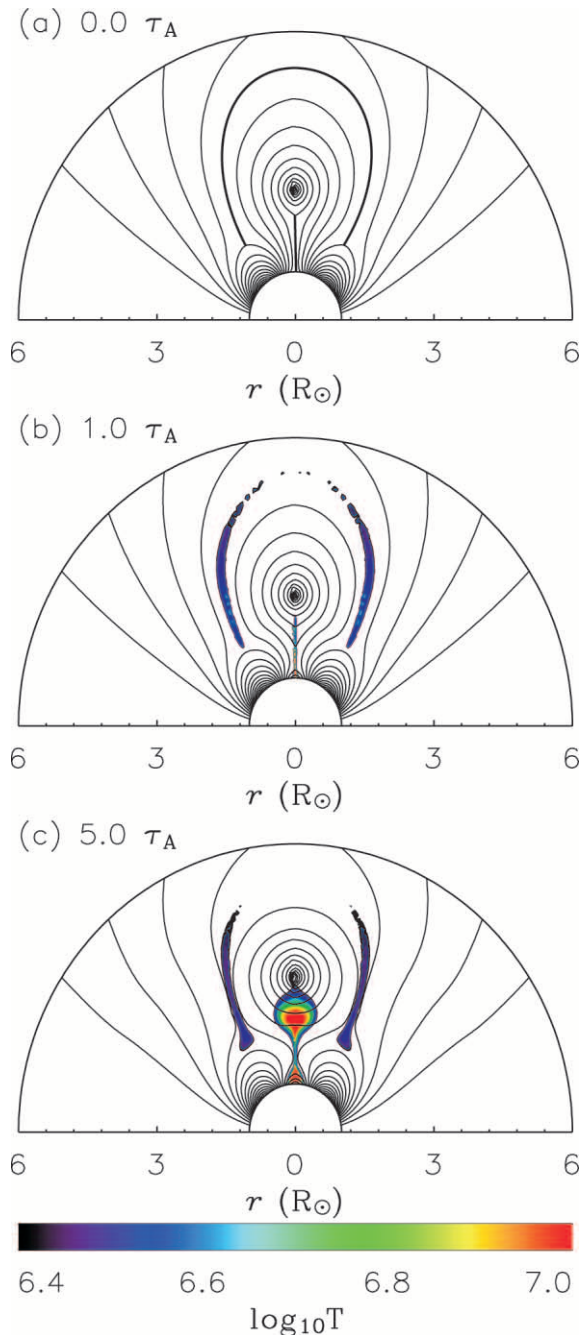


FIG. 1.—Magnetic configuration in black solid curves and temperature distribution in color at several separate times for case A, in which reconnection occurs simultaneously in the transverse and vertical current sheets. The cool blue and the hot red correspond to 2.51×10^6 and 1.0×10^7 K, respectively.

erupts upward, as shown in Figures 1b and 1c. The rope is immediately accelerated without an initial slow rising phase as shown in Figure 2 (solid line), and it gains its maximum eruption speed of 595 km s^{-1} at about $t = 5\tau_A$, when h_a reaches 2.31 (Fig. 1c). Meanwhile, a cusp-shaped structure with high temperature is clearly seen in Figure 1c, a typical feature of flares. In addition, a high-temperature structure appears in the corona right above the cusp structure at 1.5 in height.

In case B, reconnection occurs first in the transverse current sheet, and then with the growth of the current in the vertical current sheet, reconnection follows over there. Figures 3a–3c show the magnetic configuration and temperature distribution

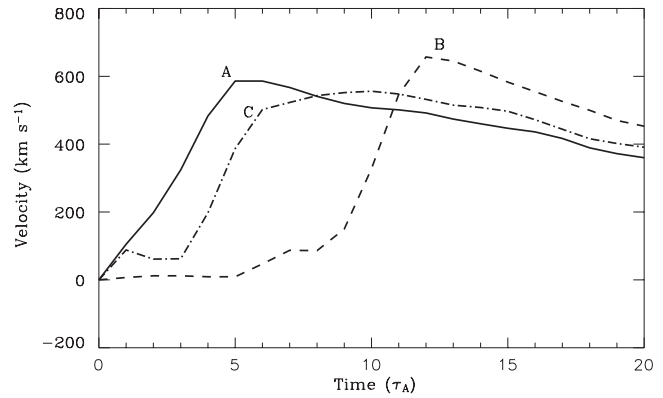


FIG. 2.—Velocity of the flux rope axis vs. time for each of the three cases: A (solid line), B (dashed line), and C (dash-dotted line).

at several separate times. At $t = 1\tau_A$, when reconnection is initiated in the transverse current sheet, the temperature along the sheet rises. As shown in Figure 2 (dashed line), the flux rope's speed increases with time very slowly until reconnection sets in across the vertical current sheet at about $t = 7\tau_A$ (Fig. 3b). Then the flux rope undergoes a slight deceleration of short duration (about $1\tau_A$), followed by a quick acceleration. The rope gains its maximum speed of 670 km s^{-1} at about $t = 12\tau_A$, when h_a reaches 2.34 (Fig. 3c). Similarly, a cusp-shaped structure with high temperature and a coronal high-temperature structure also appear in this case.

In case C, reconnection occurs first in the vertical current sheet, and then with the growth of the current in the transverse current sheet, reconnection follows over there. Figures 4a–4c show the magnetic configuration and temperature distribution at several separate times. At $t = 1\tau_A$, when reconnection occurs only in the vertical current sheet, the temperature along the sheet rises, as shown in Figure 4a. It can be seen from Figure 2 (dash-dotted line) that the flux rope is accelerated before that time, slightly decelerated afterward for about $2\tau_A$ in duration, and then accelerated again with a much larger acceleration. The flux rope gains a maximum speed of 568 km s^{-1} at about $t = 10\tau_A$, when h_a reaches 3.0 (Fig. 4c). This case differs from case B in that the cusp-shaped structure is formed much earlier: it becomes clear as early as $t = 4.7\tau_A$ (Fig. 4b), and at that time the reconnection initiates in the transverse current sheet.

In summary, magnetic reconnection causes an eruption of the flux rope and the formation of a cusp-shaped structure of high temperature in all three cases. The former is presumably a manifestation of CMEs, whereas the latter characterizes a two-ribbon flare. The reconnection sequence plays a critical role in the motion of the erupting flux rope and the formation of the cusp-shaped structure. The reconnection in the transverse current sheet is apt to produce a gradual acceleration of the flux rope but a higher peak speed and has little bearing on the formation of the cusp-shaped structure. On the other hand, the reconnection in the vertical current sheet is directly responsible for the formation of the cusp-shaped structure and leads to an immediate acceleration of the flux rope. It is interesting to note that a short-term deceleration occurs before the rapid acceleration caused by reconnection across the vertical current sheet, as seen in cases B and C. At present we do not know exactly why the flux rope has such a behavior. A possible reason might be that the magnetic pressure decreases right beneath the flux rope when reconnection starts in the vertical current sheet. High-resolution observations at both optical and radio bands

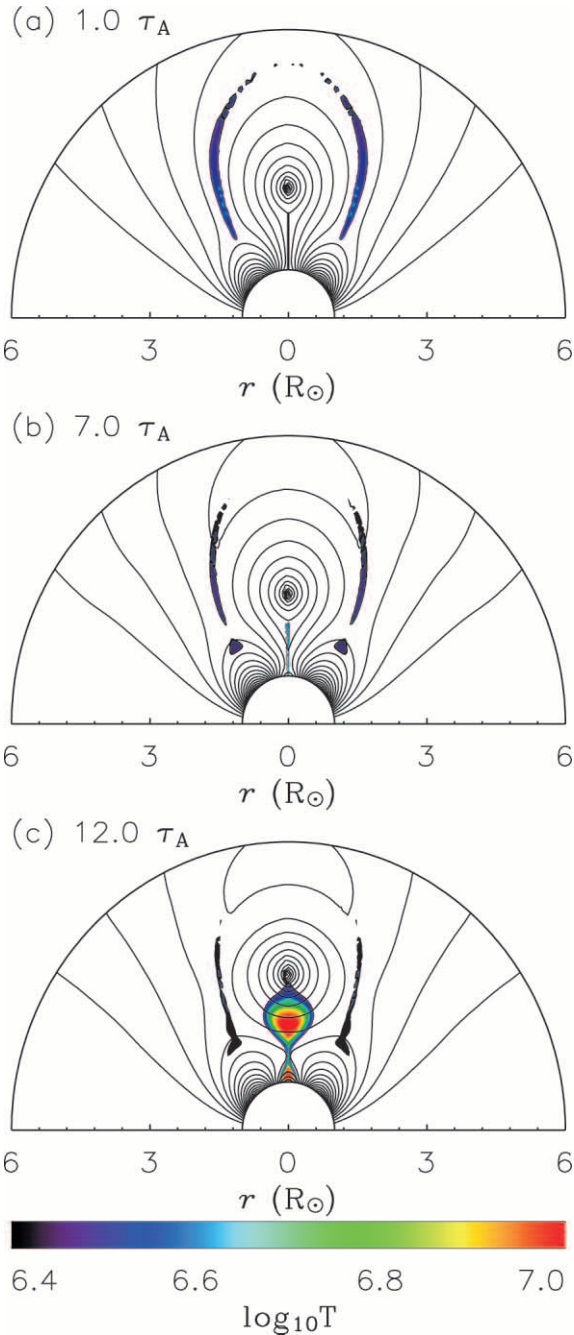


FIG. 3.—Same as Fig. 1, but for case B, in which reconnection occurs first in the transverse current sheet and then in the vertical one.

show indications that flux systems first shrink during the impulsive phases of flares and then explode later in the main phases of flares (Ji et al. 2004; Li & Gan 2005). This seems to be consistent with the simulation results of reconnection occurring in the vertical current sheet in cases B and C. More careful work needs to be done in order to judge whether this is a common behavior of flux rope dynamics in the flare impulsive phase. Incidentally, since we have not considered the background solar wind, the flux rope’s speed decreases after it obtains a peak speed in all three cases.

4. CONCLUDING REMARKS

Using time-dependent resistive MHD simulations, we find solutions associated with an isolated coronal flux rope embedded

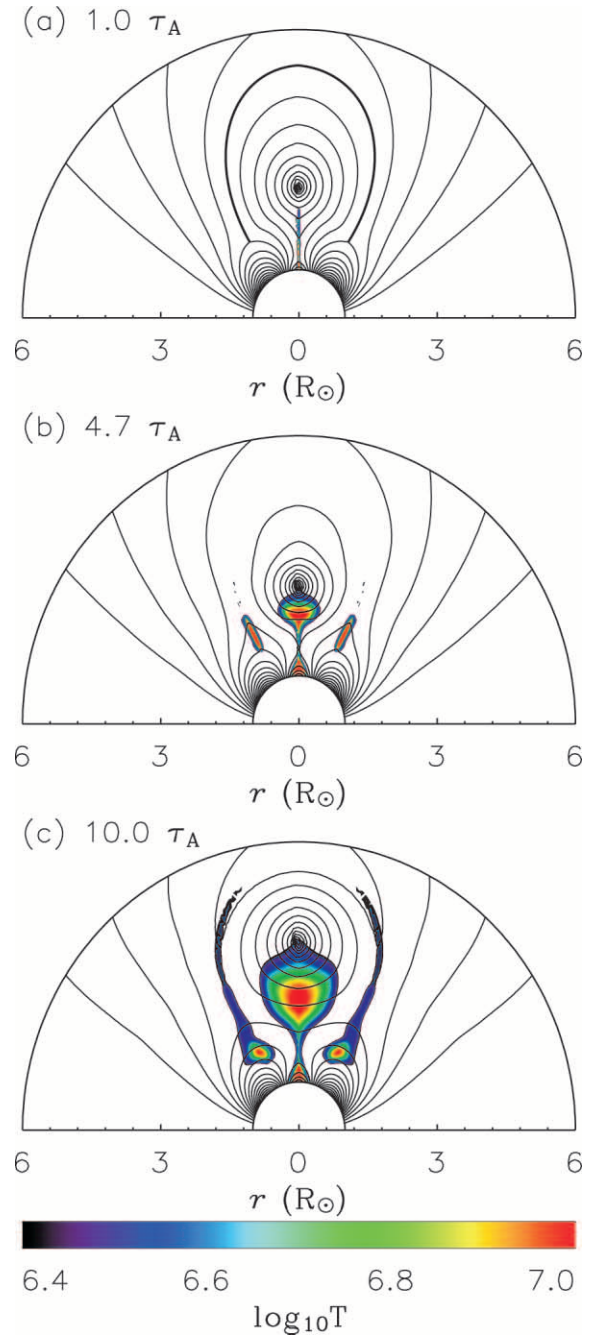


FIG. 4.—Same as Fig. 1, but for case C, in which reconnection occurs first in the vertical current sheet and then in the transverse one.

in a quadrupolar background field and accompanied by a transverse current sheet above and a vertical current sheet below the rope. Reconnection may occur in the current sheets either simultaneously or one after another. The present model agrees with the breakout model (Antiochos et al. 1999; Lynch et al. 2004) if reconnection is initiated in the transversal current sheet, and it returns to the standard flare model (Chen & Shibata 2000) if reconnection is initiated in the vertical current sheet. Nevertheless, we argue that both breakout-like external reconnections and tether-cutting internal reconnections are essential to magnetic eruption in general. Williams et al. (2005) showed observational evidence for the presence of both tether cutting and breakout in eruptive events. Our simulations just combine the two models, which is probably more relevant to observations

that many eruptive events occur in background fields of quadrupolar magnetic configuration (Sterling & Moore 2004a, 2004b; Gary & Moore 2004).

The present magnetic configuration and the dynamical evolution shed new light on understanding the relationship between CMEs and flares, which is a topic with great interest and hot debate. More and more investigations prefer a closer and rather intrinsic association between CMEs and surface activities (see Zhang et al. 2001a, 2001b; Zhou et al. 2003).

Zhang et al. (2001a) reported that the kinematic evolution of CMEs can be described in a three-phase scenario: the initiation phase, the impulsive acceleration phase, and the propagation phase. Furthermore, they found that following the initiation phase, the CME displays an impulsive acceleration phase, which starts almost simultaneously with the flare onset time. After the acceleration phase the CME undergoes a propagation phase. In addition, Zhang et al. (2001b) found a halo CME that moved slowly in the initial phase and was later on accelerated and erupted. This is consistent with our case B, in which reconnection first starts in the transversal current sheet, leading to a slow upward motion of the CME, and subsequently, because of reconnection onset in the vertical current sheet, the CME acceleration is quickened until it reaches the maximum speed. In other words, the break-out occurs first and the tether cutting follows. However, this is just one possibility; the other two cases we work out would

appear in different circumstances. Zhou et al. (2003) gave a statistical result that 59% of the selected 197 halo CMEs initiate earlier than the flare onset and 41% are preceded by flare onsets. The latter samples could relate to our case C. Furthermore, Zhang et al. (2001a) also found one CME that did not show an initiation phase but was immediately accelerated to the maximum speed. This example is very similar to our case A, in which reconnection occurs simultaneously in the two current sheets.

Another point worthy of mention relates to the effect of the reconnection sequence on the maximum speed of CMEs. The flux rope, identified as the CME here, has the largest speed when reconnection first starts in the transverse current sheet. On the other hand, the maximum speed is the lowest when reconnection first starts in the vertical current sheet. This implies that the reconnection sequence could affect the maximum speed of CMEs.

The authors are greatly indebted to the anonymous referee for helpful comments and valuable suggestions on the manuscript. Y. Z. Z. thanks J. Y. Ding for kind assistance in coding and P. F. Chen for helpful discussions. This work is supported by the National Natural Science Foundation of China (10233050 and 40274049) and the National Key Basic Science Foundation (TG2000078404).

REFERENCES

- Amari, T., Luciani, J. F., Mikic, Z., & Linker, J. 2000, *ApJ*, 529, L49
 Antiochos, S. K., DeVore, C. R., & Klimchuk, J. A. 1999, *ApJ*, 510, 485
 Anzer, U. 1978, *Sol. Phys.*, 57, 111
 Chen, J., et al. 1997, *ApJ*, 490, L191
 Chen, P. F., & Shibata, K. 2000, *ApJ*, 545, 524
 Cheng, J. X., Fang, C., Chen, P. F., & Ding, M. D. 2005, *Chinese J. Astron. Astrophys.*, 5, 265
 Dere, K. P., Brueckner, G. E., Howard, R. A., Michels, D. J., & Delaboudiniere, J. P. 1999, *ApJ*, 516, 465
 Forbes, T. G. 2000, *J. Geophys. Res.*, 105, 23153
 Forbes, T. G., & Isenberg, P. A. 1991, *ApJ*, 373, 294
 Forbes, T. G., & Priest, E. R. 1995, *ApJ*, 446, 377
 Gary, G. A., & Moore, R. L. 2004, *ApJ*, 611, 545
 Heyvaerts, J., Priest, E. R., & Rust, D. M. 1977, *ApJ*, 216, 123
 Hirayama, T. 1974, *Sol. Phys.*, 34, 323
 Hu, Y. Q. 1989, *J. Comput. Phys.*, 84, 441
 ———. 2004, *ApJ*, 607, 1032
 Hu, Y. Q., Li, G. Q., & Xing, X. Y. 2003, *J. Geophys. Res. Space Phys.*, 108, 1072
 Hu, Y. Q., & Liu, W. 2000, *ApJ*, 540, 1119
 Isenberg, P. A., Forbes, T. G., & Démoulin, P. 1993, *ApJ*, 417, 368
 Ji, H., Wang, H., Goode, P. R., Jiang, Y., & Yurchyshyn, V. 2004, *ApJ*, 607, L55
 Li, Y. P., & Gan, W. Q. 2005, *ApJ*, 629, L137
 Lin, J., & Forbes, T. G. 2000, *J. Geophys. Res.*, 105, 2375
 Lin, J., Forbes, T. G., & Isenberg, P. A. 2001, *J. Geophys. Res.*, 106, 25053
 Low, B. C. 1996, *Sol. Phys.*, 167, 217
 ———. 2001, *J. Geophys. Res.*, 106, 25141
 Lynch, B. J., Antiochos, S. K., MacNeice, P. J., Zurbuchen, T. H., & Fisk, L. A. 2004, *ApJ*, 617, 589
 Mikić, Z., & Linker, J. 1994, *ApJ*, 430, 898
 Moore, R. L., Sterling, A. C., Hudson, H. S., & Lemen, J. R. 2001, *ApJ*, 552, 833
 Priest, E. R. 1988, *ApJ*, 328, 848
 Shibata, K. 1999, *Ap&SS*, 264, 129
 Shibata, K., Masuda, S., Shimojo, M., Hara, H., Yokoyama, T., Tsuneta, S., Kosugi, T., & Ogawara, Y. 1995, *ApJ*, 451, L83
 Sterling, A. C., & Moore, R. L. 2004a, *ApJ*, 602, 1024
 ———. 2004b, *ApJ*, 613, 1221
 Sturrock, P. A. 1966, *Nature*, 211, 695
 Sturrock, P. A., Kaufman, P., Moore, R. L., & Smith, D. F. 1984, *Sol. Phys.*, 94, 341
 Török, T., & Kliem, B. 2005, *ApJ*, 630, L97
 Tsuneta, S. 1997, *ApJ*, 483, 507
 Wang, J., et al. 2005, *Chinese J. Astron. Astrophys.*, in press
 Williams, D. R., Török, T., Démoulin, P., van Driel-Gesztelyi, L., & Kliem, B. 2005, *ApJ*, 628, L163
 Wood, B. E., Karovska, M., Chen, J., Brueckner, G. E., Cook, J. W., & Howard, R. A. 1999, *ApJ*, 512, 484
 Wu, S. T., Guo, W. P., & Dryer, M. 1997, *Sol. Phys.*, 170, 265
 Zhang, J., Dere, K. P., Howard, R. A., Kundu, M. R., & White, S. M. 2001a, *ApJ*, 559, 452
 Zhang, J., Wang, J. X., & Nitta, N. 2001b, *Chinese J. Astron. Astrophys.*, 1, 85
 Zhang, Y. Z., Hu, Y. Q., & Wang, J. X. 2005, *ApJ*, 626, 1096
 Zhou, G. P., Wang, J. X., & Cao, Z. L. 2003, *A&A*, 397, 1057
 Zhou, G. P., Wang, J. X., & Zhang, J. 2006, *A&A*, 445, 1133